buildings

MDPI

Article

Enhancement of Mechanical Properties, Wettability, Roughness, and Thermal Insulation of Epoxy–Cement Composites for Building Construction

Saif M. Jasim [1], Nadia A. Ali [2], Seenaa I. Hussein [2], Areej Al Bahir [3], Nashaat S. Abd EL-Gawaad [4], Ahmed Sedky [5], Abdelazim M. Mebed [6] and Alaa M. Abd-Elnaiem [5,*]

[1] Physics Department, College of Science, Nahrain University, Baghdad 64074, Iraq; saif.muhammed@nahrainuniv.edu.iq
[2] Physics Department, College of Science, Baghdad University, Baghdad 10071, Iraq; nadia.ali@sc.uobaghdad.edu.iq (N.A.A.); seenaa.hussein@sc.uobaghdad.edu.iq (S.I.H.)
[3] Chemistry Department, Faculty of Science, King Khalid University, Abha 64734, Saudi Arabia; areeej@kku.edu.sa
[4] Muhayil Asir, Applied College, King Khalid University, Abha 62529, Saudi Arabia; nshat@kku.edu.sa
[5] Physics Department, Faculty of Science, Assiut University, Assiut 71516, Egypt; sedky1@aun.edu.eg
[6] Department of Physics, College of Science, Jouf University, P.O. Box 2014, Sakaka 72311, Saudi Arabia; amali@ju.edu.sa
* Correspondence: abd-elnaiem@aun.edu.eg; Tel.: +20-1151159892

Abstract: In this study, epoxy–cement composites with different concentrations of cement nanofiller and ~67.5 nm in size (0, 5, 10, 15, and 20 wt%) were synthesized using the solution casting method. The epoxy–cement composites' structural, mechanical, wettability, roughness, and thermal insulation were investigated. The synthesized epoxy resin is amorphous, whereas epoxy–cement composites are crystalline, and its crystallinity depends on the filler ratio. The incorporated cement hindered the spread of cracks and voids in the composite with few illuminated regions, and the epoxy/cement interface was identified. The Shore D hardness, impact strength, and flexural strength gradually increased to 92.3, 6.1 kJ/m^2, and 40.6 MPa, respectively, with an increase in the cement ratio up to 20 wt%. In contrast, the incorporation of a cement ratio of up to 20 wt% reduced thermal conductivity from 0.22 to 0.16 W/m·K. These findings indicated that resin and cement nanoparticle fillers affected the chemical composition of epoxy, which resulted in high molecular compaction and thus strong mechanical resistance and enhanced thermal insulation. The roughness and water contact angle (WCA) of epoxy increased by increasing the cement nanofiller. In contrast, the surface energy (γ) of a solid surface decreased, indicating an inverse relation compared to the behavior of roughness and WCA. The reduction in γ and the creation of a rough surface with higher WCA can produce a suitable hydrophobic surface of lower wettability on the epoxy surface. Accordingly, the developed epoxy–cement composites benefit building construction requirements, among other engineering applications.

Keywords: epoxy–cement; concrete; wettability; roughness; mechanical; thermal conductivity; building construction

check for updates

Academic Editors: Shengwen Tang and Peng Zhang

Received: 11 December 2024
Revised: 3 January 2025
Accepted: 6 February 2025
Published: 19 February 2025

Citation: Jasim, S.M.; Ali, N.A.; Hussein, S.I.; Al Bahir, A.; Abd EL-Gawaad, N.S.; Sedky, A.; Mebed, A.M.; Abd-Elnaiem, A.M. Enhancement of Mechanical Properties, Wettability, Roughness, and Thermal Insulation of Epoxy–Cement Composites for Building Construction. *Buildings* **2025**, *15*, 643. https://doi.org/10.3390/buildings15040643

Copyright: © 2025 by the authors. Licensee MDPI, Basel, Switzerland. This article is an open access article distributed under the terms and conditions of the Creative Commons Attribution (CC BY) license (https://creativecommons.org/licenses/by/4.0/).

1. Introduction

Polymer films are optically transparent, but they are thermal and electrical insulators [1–3]. In addition, polymers have poor mechanical properties; therefore, more attention has been directed to improving their thermal, electrical, and mechanical properties [4,5].

Improvement in the mechanical properties and thermal insulation of a polymer is highly required for building construction.

The incorporation of nanofillers into a polymer, such as carbon nanotubes, multi-walled carbon nanotubes, graphene, graphene oxide, and zinc oxide nanoparticles, usually increases their physicochemical characteristics [6–8]. However, the properties of modified polymer composites are influenced by the type, concentration, size, and shape of the incorporated materials [9,10]. The incorporation of new components into polymers usually has advantages and disadvantages. For example, carbon-based nanomaterials enhance the mechanical, electrical, and thermal properties of the polymer, but they impair its optical transparency [2,11]. In addition, considering the cost-effectiveness of incorporated materials is particularly needed for large-scale development and industry. Accordingly, the usage of cheap and plentiful materials, such as cement, concrete, fly ash cenospheres, date palms, etc., to improve the mechanical and thermal characteristics of polymers is beneficial for building construction and other engineering applications [12–16]. Generally, polymer-based materials have been employed in environments such as underwater concrete or reactive particle concrete, which, in some cases, are better than ceramics, to meet practical applications [17]. Concrete is efficiently suited for enhancing the properties of polymer materials because its composition can be modified quite simply [18]. Polymer–cement concretes have promising properties, such as high tensile and high flexural strength, as well as adherence to a variety of substrates, tightness, and resistance to some chemical attacks [19]. Polymer–cement composites are being used in the repair and protection of concrete structures; the construction of pavements, including industrial floors; and the manufacture of pre-cast parts [20].

Recently, epoxy–cement composites have received a lot of interest in the realm of civil engineering [21]. Epoxy resins have revealed excellent properties, such as high strength and durability, low cure shrinkage, adhesion, compatibility with a wide range of materials, electrical insulation, corrosion, and chemical resistance [22]. Epoxy–cement composites can be used in load-bearing structures, such as beams, columns, and slabs, due to their enhanced mechanical properties (e.g., flexural strength, impact resistance). On the other hand, cement nanoparticles are usually used as a binding medium due to their physical and chemical properties [17]. The inclusion of cement or concrete nanoparticles into an epoxy medium to form an epoxy–concrete composite demonstrated a considerable loss of strength due to the thermo-oxidative deterioration of the epoxy and de-bonding between aggregates and the binder [23]. Cement can harden into a high-strength matrix after combining with aggregate and going through a hydration process [24]. The epoxy plastic plates can be reused by inserting them into concrete to ensure the strength of epoxy resin concrete [25]. Concrete's diminishing durability poses major hazards to building structure safety [26]. Moreover, damage such as erosion and fractures has frequently occurred at stress concentration places and cyclic deformation zones, resulting in dangers and possible harm to concrete structures [27]. One of the common modification methods is to incorporate polymer as a co-binder into concrete, making it more susceptible to changes in performance [28,29]. The choice of cement nanoparticles as a filler material was driven by their cost-effectiveness, compatibility with epoxy, self-healing properties, and suitability for building construction applications. While CNTs and graphene offer exceptional properties, they are less practical for large-scale construction due to their high cost and processing challenges. Cement nanoparticles provide a balanced combination of mechanical, thermal, and surface properties, making them an ideal choice for enhancing the performance of epoxy composites in construction.

The analysis of the microstructure of polymer-based composites is required to understand the interaction between polymer and cement and investigate their interface to develop polymer properties [30]. Concrete repair and reinforcement are critical for extending the structures' service life, with urban growth slowing and infrastructure steadily improving in terms of maintenance and reinforcement [31]. Therefore, achieving high-performance buildings using polymeric composite materials is critical. However, there are still a lot of issues for controlling the microstructure of polymer/cement composites to improve matrix ductility [32]. The fineness of cement is determined by its particle size, as the cement hydration rate is proportional to particle size [33]. Further investigations have revealed that epoxy resin concrete is widely used in building structural reinforcements [34]. Epoxy resin adhesive has major applications in the field of concrete and is extensively used in the repair of concrete members, bridge engineering, runway repair, road repair, and structural fracture reinforcement [35]. In addition, epoxy resin is commonly used in bridge construction to withstand high stresses [36].

The value of thermal conductivity (K), thermal diffusivity, and specific heat of epoxy composites was reduced by increasing the incorporation of date palm up to 30 wt%, with a minimum K value of 0.14 W/m·K [14]. The improved thermal insulation properties of these composites make them suitable for energy-efficient building materials, reducing heat transfer and improving energy savings. The thermal conductivity and thermal diffusivity of epoxy increased by increasing the silicon carbide ratio in the range of 0–3 wt%, as well as by boosting the operating temperature [37]. The thermal expansion of epoxy mortar composites showed a small rise with a polymer ratio up to 15 wt% and subsequently increased dramatically with a higher polymer ratio; however, permeability and thermal conductivity showed an opposite sequence [38]. In contrast, the inclusion of graphene, Cu, or $CaCO_3$ nanoparticles reduced the thermal expansion of epoxy while increasing the thermal conductivity [6,39]. The mechanical characteristics and thermal conductivity of cement foam incorporating epoxy polymer at a ratio of 0–9 wt% were investigated. The epoxy ratio significantly increases thermal conductivity while decreasing mechanical properties such as plastic viscosity and yield stress [40]. Similarly, epoxy–concrete composites with polymer content ratios ranging from 6 to 16 wt% are thermally treated to increase mechanical properties such as Young modulus, shear modulus, strength, compressive strength, and flexural strength [23]. Epoxy–cement has been further developed with various nanofillers, such as Nb and Zr nanoparticles, for bioactivity applications [41]. The addition of cement nanoparticles, like other fillers, to polymers should be carefully chosen to boost or reduce mechanical and thermal properties. For example, the impact strength and Shore A hardness of acrylic polymer increased with an increase in the cement filler ratio up to 2 wt% and 4 wt%, respectively, while decreasing with further filler ratio increase [24].

Roughness, water contact angle (WCA), or water wettability are fundamental aspects of medical device biocompatibility, printing on paper, structural integrity in additive manufacturing, and surfaces after abrasive processing [42,43]. The evaluation of WCA for epoxy is useful for evaluating the modification in surface properties due to the addition of cement nanofiller [44,45]. There are two methods to measure the WCA; the first is the Wenzel state, whereas the second is the Cassie–Baxter state. The Wenzel model is demonstrated by the drop of water falling on the solid surface, while the Cassie–Baxter model deals with the drop of water rolling off on the solid surface to determine the ability of self-cleaning [46,47]. Currently, it has been shown that the surface roughness and WCA of epoxy vary with cement nanofiller. In addition, WCA can be used to determine the surface energy of a solid surface (γ), the energy per unit area of an exposed surface of a liquid. The hydrophobic nature and enhanced wettability of epoxy–cement composites make them ideal for protective coatings, self-cleaning surfaces, and water-resistant applications in

construction. The composites offer improved resistance to environmental factors, such as moisture, chemicals, and temperature fluctuations, making them durable and sustainable alternatives to traditional building materials.

Nowadays, modifying polymer materials is commonly done to accomplish building materials engineering. In addition to being designed for usage in harsh environments, recycled concrete is especially well suited for the modification of polymer materials because its composition can be readily altered, and admixtures are already a part of contemporary concrete. Therefore, in this study, epoxy–cement composites with cement ratios of 5, 10, 15, and 20 wt% were synthesized using the solution casting method. The structural, mechanical, and thermal properties of epoxy–cement composites are investigated using various analytical techniques. The derived results were compared with existing literature, demonstrating that the incorporation of cement nanoparticles into an epoxy matrix improves its structural, mechanical, and thermal properties, making it appropriate for building construction.

2. Materials and Methods

Epoxy was purchased from the Swiss Chemical Company in Egypt. The epoxy has a density of 1.1 g/cm^3 and a viscosity range of 3–5 poise at 25 °C. Ordinary Portland cement (OPC) powder was purchased from Al Gurg Fosroc LLC, Dubai, UAE. The OPC consists of 63 wt% calcium oxide (CaO), 21.9 wt% silicon dioxide (SiO_2), 6.9 wt% aluminum oxide (Al_2O_3), 3.9 wt% iron oxide (Fe_2O_3), 2.5 wt% magnesium oxide (MgO), and 1.7 wt% sulfur trioxide (SO_3). The particle size and particle distribution of purchased cement powder were determined using an atomic force microscopy (AFM) instrument, model AFM-AA3000/220V, from Angstrom Advanced, Inc., Methuen, MA, USA.

Pure epoxy and epoxy–cement composites were synthesized using the solution casting method. The hardener liquid was gradually added to the epoxy resin at room temperature (RT ≈ 25 °C) with a stoichiometric volume ratio of 1:2. The mixture was physically mixed at RT for 3 min using a mixing stick. For epoxy–cement composites, cement was added as a filler in ratios of 5, 10, 15, and 20 wt% to the epoxy resin using a high-speed continuous magnetic stirrer. The mixture was then poured into a stainless-steel mold and allowed to dry at RT for 24 h. The molds varied in size and dimensions depending on the desired tests. For example, for the thermal conductivity test, the mold and resulting sample were cylindrical, with a diameter of 1.5 cm and a thickness of 1.5 cm. Molds and samples for impact strength, flexural strength, and hardness tests are rectangular, with dimensions of 5.5 cm × 1 cm × 0.3 cm, 8 cm × 8 cm × 40 cm, and 1.5 cm × 1.5 cm × 0.6 cm, respectively. A silicon-based release agent was used in the mold to simplify the extraction of the composite samples. Each synthesized sample was allowed to dry for 1 h and then left for an additional 24 h before testing to ensure cohesive curing.

A wide-angle X-ray diffraction (XRD) instrument, model Bruker D-8, operated at 45 kV and 30 mA was used to investigate the phase purity and crystalline structure of the samples. A Cu-Kα anode was employed as the X-ray source with a wavelength of 1.5406 Å. The XRD patterns were recorded with a step size of 0.1° and a scan speed of 0.2 °/s over a diffraction angle (2θ) range of 20° to 80°. A scanning electron microscopy (SEM) instrument, model FEI Inspect S50, operated at 15 kV or 30 kV, was used to examine the surface morphology of the samples. The SEM system was equipped with energy-dispersive X-ray (EDX) spectroscopy and EDX mapping capabilities operated by Bruker Nano GmbH, Germany, at a voltage of 15 kV.

The Shore D hardness was measured using a digital hardness tester with a scale range of 0 and 100 units. The indenter was affixed to the sample's surface using a durometer, and the highest recorded reading was taken as the hardness value [48]. The impact strength ($I.S$) was calculated using the formula [49] $I.S = \frac{U_c}{A}$, where U_c is the fracture energy, and A is the cross-sectional area. The flexural strength (σ) was determined using a three-point bending test with a rectangular shape sample, as illustrated in Figure 1a. The flexural strength was estimated using the formula [50] $\sigma = \frac{3FL}{2bd^2}$, where b and d are the width and depth of the sample, F is the applied load at the fracture point, and L is the span length, as shown schematically in Figure 1a.

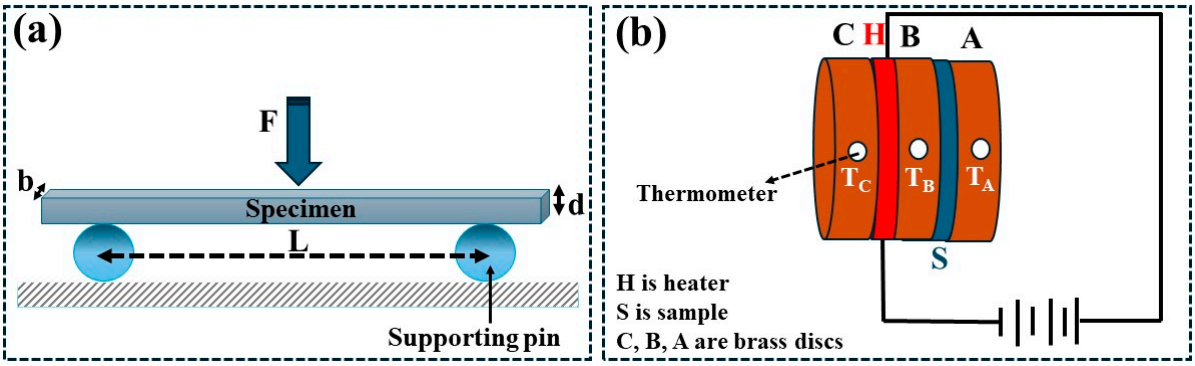


Figure 1. Schematic images of (**a**) flexural strength test and (**b**) Lee's disk experiment.

Lee's disc apparatus, schematically illustrated in Figure 1b, was used to determine thermal conductivity (K) for the specimens studied [51,52]. The temperatures of the brass discs A, B, and C, denoted as T_A, T_B, and T_C, were measured using a digital thermometer after thermal equilibrium was achieved. The heater was operated at a voltage of 6 V and a current of 0.25 A. The numerical value of K was calculated using the formula [53] $K = \frac{\varepsilon[T_A + \frac{2}{r}(d_A + \frac{d_s}{4})T_A + \frac{d_s T_B}{2r}]}{(\frac{T_B - T_c}{d_s})}$. The parameter ε represents the thermal energy transfer per unit area of the disc in seconds and is given by [35,39] $\varepsilon = \frac{IV}{\pi r^2(T_A - T_B) + 2\pi r[d_A T_A + \frac{d_s(T_A - T_B)}{2} + d_B T_B + d_c T_c]}$, where r is the radius of the disc; d_A, d_B, and d_c are the thicknesses of the brass discs A, B, and C, respectively; and d_s is the thickness of the sample.

The surface roughness of the samples was measured using a surface roughness tester (TR-100), which quantifies surface texture. Roughness is defined as the vertical deviation of a physical surface from its ideal smooth form. It is routinely evaluated and plays a critical role in various processes, such as friction and adhesion. The WCA between the sample and water, as a liquid, was determined. The WCA of the acrylic polymer/cement nanocomposites was measured using the sessile drop method with a Kyowa contact angle meter (Model DME 211, Niiza, Saitama, Japan). On a smooth sample surface, the WCA was measured at intervals of 45–60 s. Each measurement was recorded at predetermined intervals and saved as an image.

3. Results and Discussion

3.1. Structural Properties

Figure 2a shows the optical image of the cement nanopowder, which exhibits a fine powder with a green-grey color. The 2D AFM image and the granularity normal distribution chart of cement nanoparticles are depicted in Figure 2b and Figure 2c, respectively. The 3D AFM image for comparable cement nanofillers is available elsewhere [24]. The 2D AFM image shows that the cement nanoparticles are uniform in both size and distribution. The granularity normal distribution chart shows a Gaussian distribution for cement particle size

around the average value, which is common for most AFM analyses [25]. The estimated range of particle sizes is between 42.5 and 100 nm, while the average particle size of cement was approximately 67.5 nm.

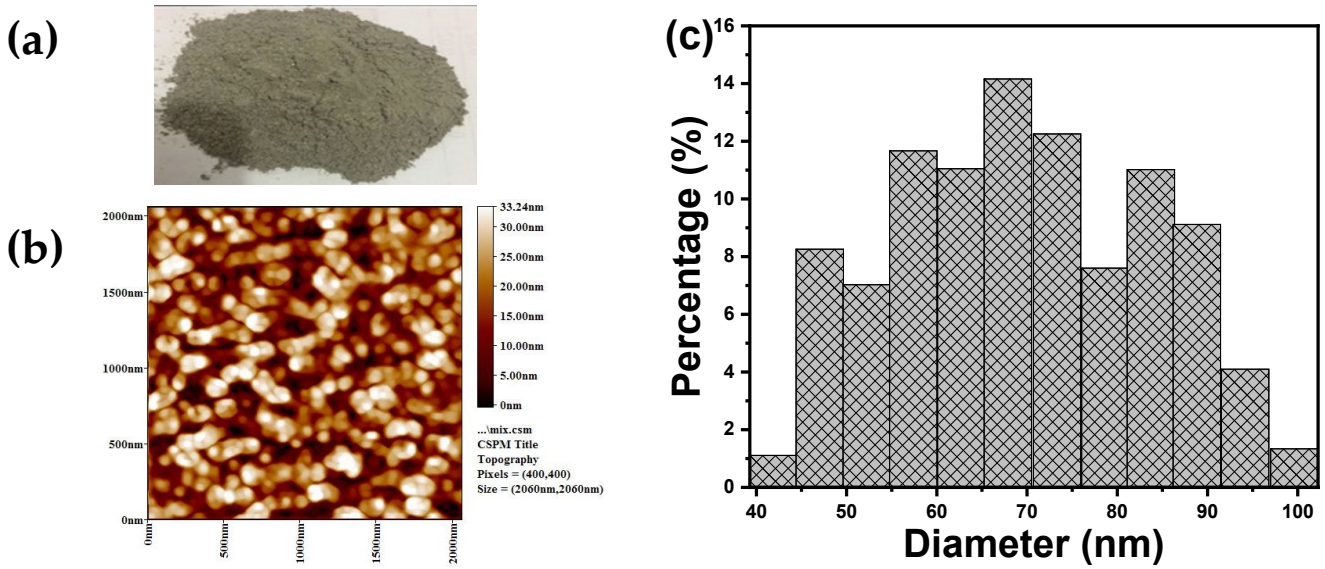


Figure 2. (**a**) Optical image of cement powder, (**b**) 2D AFM image, and (**c**) granularity normal distribution chart of cement nanoparticles.

Figure 3 shows the EDX charts and EDX mapping of epoxy and epoxy–cement composites. The bonding between the epoxy resin and hydroxyl ions is demonstrated in the SEM and EDX mapping. The circles of different colors that appear in the SEM images of epoxy and epoxy–cement composites represent C and Al, selected as examples of the mentioned elements in Table 1. Table 1 summarizes the weight ratio (wt%) and atomic percentage (at.%) of all detected elements in epoxy resin and epoxy–cement composites. As listed in Table 1, elements like Zr, Nb, Ru, and O, ordered by their weight ratio, appear alongside the dominant C element. The ratio of C is 68.56 wt% for pure epoxy, while the remaining elements constitute 31.44 wt%. The ratio of C decreases to 14.87 wt% and 12.97 wt% for epoxy–cement composites containing 5 wt% and 20 wt% cement, respectively. In addition, Zr, Nb, Ru, and O disappear completely and are replaced by elements such as Sb, Rb, Ca, Mo, Si, and Al in epoxy-5 wt% cement composites. Additional elements such as Ru, Pt, and K, with ratios of 4.47, 8.76, and 1.18 wt%, respectively, are observed when the cement ratio increases to 20 wt%. These elements are critical components contributing to the self-healing capacity of epoxy resin and epoxy–cement nanocomposites [54]. However, the new elements formed in the composites may explain the differences in the mechanical and thermal behaviors between epoxy and epoxy–cement composites. A similar EDX investigation for Portland cement has confirmed the presence of Ca, Si, Al, Mg, C, and O components in other studies [41].

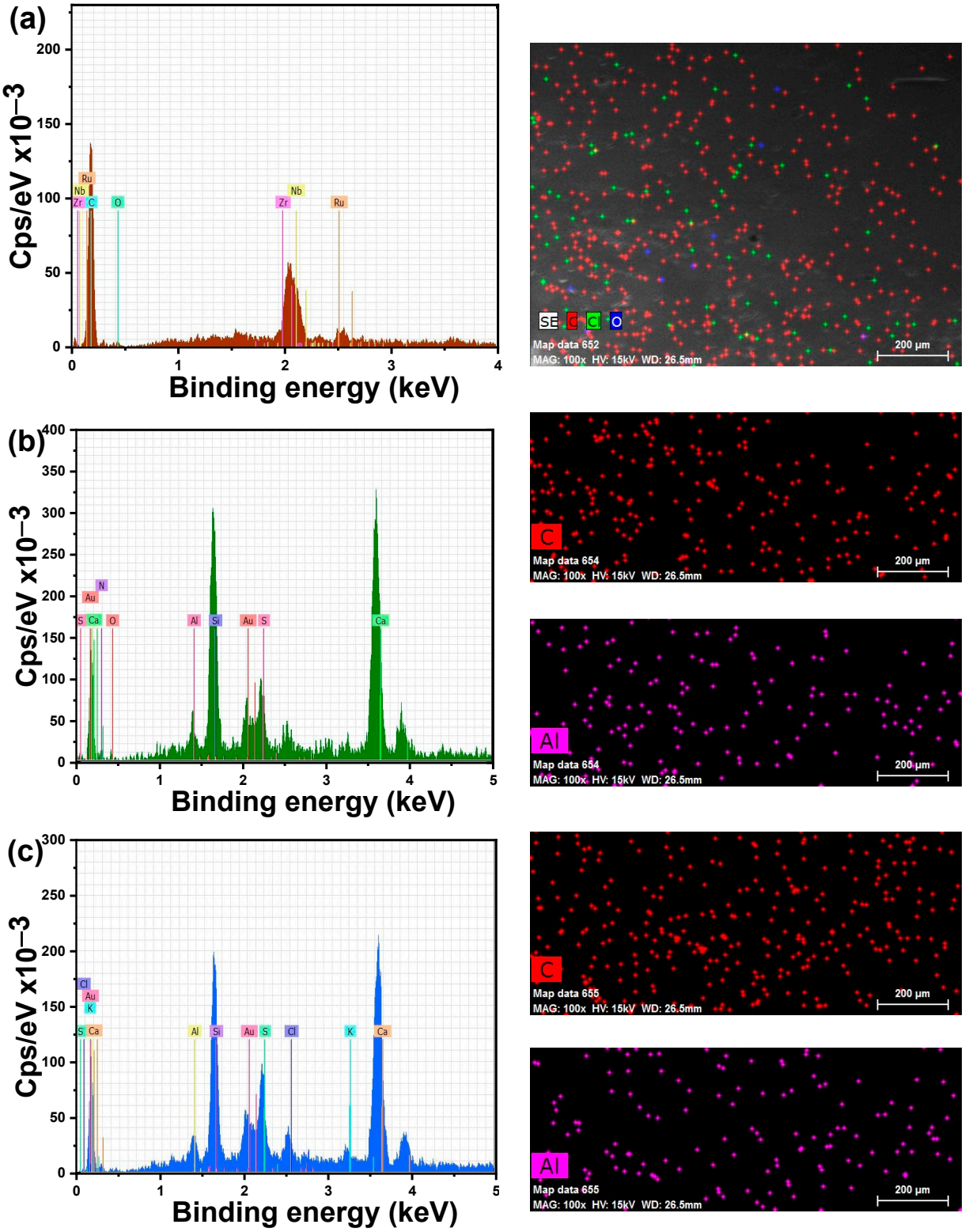


Figure 3. DX charts (**left side**) and EDX mapping (**right side**) of (**a**) epoxy resin, (**b**) epoxy-5 wt% cement composite, and (**c**) epoxy-20 wt% cement composite.

Table 1. Weight ratio (wt%) and atomic percentage (at.%) of neat epoxy, epoxy-5 wt% cement composite, and epoxy-20 wt% cement composite extracted from EDX.

Element	Pure Epoxy		Epoxy-5 wt% Cement		Epoxy-20 wt% Cement	
	wt%	at.%	wt%	at.%	wt%	at.%
C	68.56	93.25	14.87	50.51	12.97	47.93
Zr	14.46	2.59	-	-	-	-
Nb	12.30	2.16	-	-	-	-
Ru	3.23	0.52	-	-	4.47	1.96
O	1.45	1.48	-	-	-	-
Sb	-	-	31.93	10.70	24.82	9.04
Rb	-	-	25.65	12.24	18.88	9.80
Ca	-	-	10.88	11.07	9.04	10.01
Mo	-	-	8.59	3.65	12.19	5.64
Si	-	-	6.18	8.98	5.74	9.07
Al	-	-	1.89	2.85	1.95	3.21
Pt	-	-	-	-	8.76	1.99
K	-	-	-	-	1.18	1.34

Figure 4 illustrates the XRD charts of epoxy resin and epoxy–cement composites with cement ratios of 5 wt% and 20 wt%. It is well known that strong XRD patterns with a few lines indicate a high-crystalline nature, whereas weaker patterns with more lines emphasize a lower-crystalline nature [55]. The XRD pattern of pure epoxy shows no sharp peak, and there is only a broad hump located at 25°, which is attributed to the diffused cured epoxy network and confirms its amorphous nature [56]. The XRD pattern of epoxy–cement composites revealed multiple diffraction peaks, which were ascribed to their low-crystalline nature. The detected XRD peaks might be attributed to cement products and compounds between the epoxy and cement. For example, epoxy–cement composites exhibit several diffraction peaks located at 2θ = 26.5, 29.4, 30.0, 32.1, 32.4, 34.5, 36.5, 36.8, 39.5, 41.2, 42.5, 45.9, 50.2, 54.7 and 56.1°, demonstrating the formation of the calcium silicate (Ca_3SiO_5) phase (ICDD: 00-031-0301) [41]. According to the ICDD card, the Ca_3SiO_5 phase has a triclinic crystal structure and a space group of P1. Other XRD peaks could be ascribed to hydration products, such as $Ca(OH)_2$, and are observed at 2θ = 34.3, 47.2, 51.5, 54.6, 63.4, and 64.4° [57]. In general, the intensity of the XRD peaks of epoxy–cement composites is lower than that of traditional cement mortar [56]. Also, the intensity of some XRD peaks decreases as a result of decreasing the amount of $Ca(OH)_2$ with an increase in cement ratio from 5 wt% to 20 wt%. The decrease in the amount of $Ca(OH)_2$ can be attributed to the reaction of hydroxide ions, which function as catalysts for epoxy hardening; therefore, the amount of unhardened epoxy resin increases at high epoxy–cement ratios. Non-crystalline or amorphous silicate minerals react strongly with $Ca(OH)_2$ generated by cement hydration, forming additional calcium silicate hydrate gels [58,59].

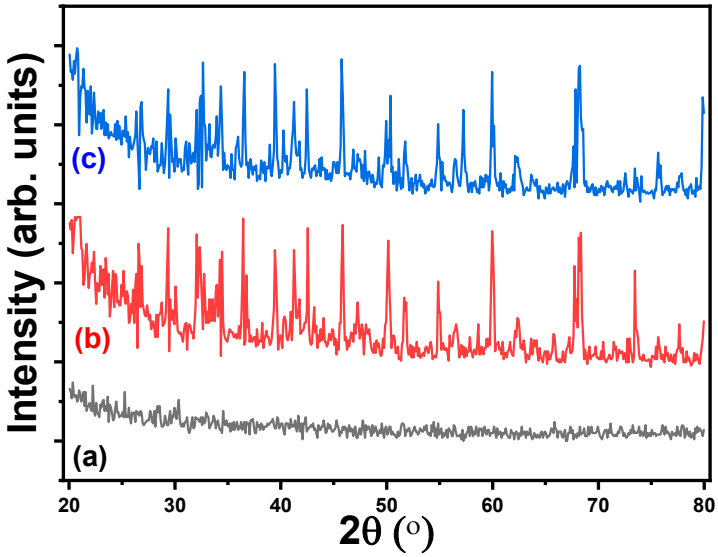


Figure 4. XRD patterns of (**a**) pure epoxy, (**b**) epoxy-5 wt% cement composite, and (**c**) epoxy-20 wt% cement composite.

Figure 5 depicts the SEM images of epoxy resin and epoxy–cement composites. Pure epoxy exhibits a smooth surface, whereas epoxy–cement composites show a rough surface. The SEM images for pure epoxy reveal the formation of the spatially cross-linked structure resulting from the chemical interaction of epoxy with the hardener. The SEM images also show some voids in pure epoxy that are reduced with the addition of cement nanoparticles. Increasing the filler ratio results in a more homogeneous distribution, consistent with previous research [23]. The morphology of cement nanoparticles within the polymer matrix (epoxy–cement composite) is more heterogeneous, particularly when the epoxy concentration is low. Lumps and discontinuous fragments of hardened resin are also observed. In general, the morphology of epoxy-based composites is dependent on numerous aspects, such as the epoxy-to-filler ratio, curing temperature, preparation process, etc. [8,17,35]. For instance, as the amount of epoxy modifier increases, the structure of the cured resin becomes more homogeneous, resulting in the formation of a more continuous polymer film [60]. The observed grains in the epoxy resin samples are exceedingly thin, leaving no gaps or illuminated patches in the matrix. The illuminated and dark zones in the SEM images of epoxy–cement composites could indicate the formation of two distinct phases, consistent with the XRD analysis. The crystal structure and morphology investigation show a gradual improvement in epoxy properties after cement incorporation, which is expected to enhance the mechanical and electrical properties of epoxy–cement composites. In this study, the SEM images of pure epoxy (Figure 5a) clearly demonstrate these characteristics, showing a flat, featureless surface with no visible particles, agglomerations, or phase separations. This smooth morphology is indicative of a well-dispersed and homogeneous epoxy matrix, which is critical for achieving optimal mechanical and thermal properties.

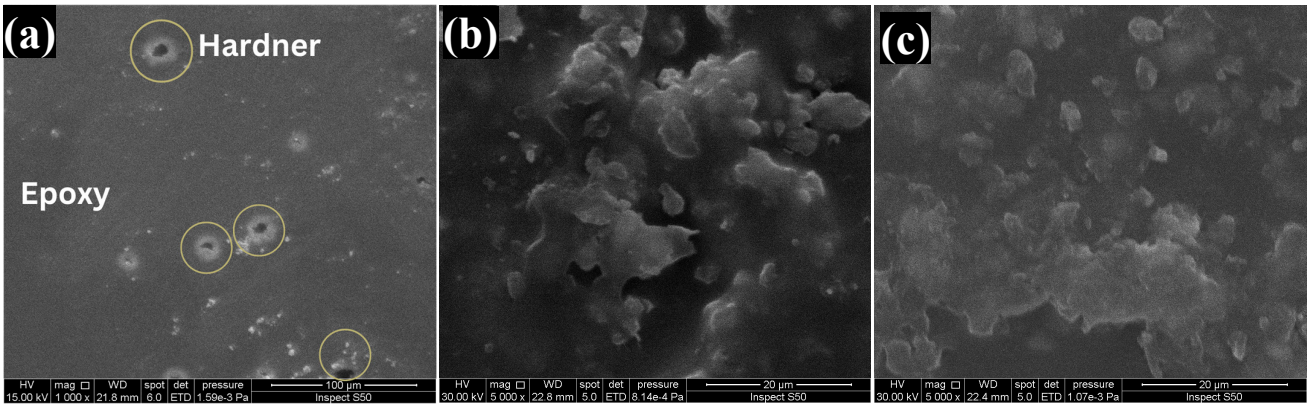


Figure 5. SEM images of (**a**) epoxy resin, (**b**) epoxy-5 wt% cement composite, and (**c**) epoxy-20 wt% cement composite.

The SEM images reveal that the cement nanoparticles are well dispersed within the epoxy matrix, indicating strong interfacial adhesion. This is evidenced by the absence of visible gaps or cracks at the epoxy–nanoparticle interface. The improved adhesion is attributed to the chemical interaction between the epoxy resin and the hydroxyl groups on the surface of the cement nanoparticles, which enhances the mechanical properties of the composites. The SEM image (Figure 5a) shows a smooth and homogeneous surface, characteristic of a well-cured epoxy matrix with minimal defects. At lower cement content (5 wt%), the surface becomes slightly rougher, with visible nanoparticles embedded in the epoxy matrix (Figure 5b). At higher cement content (20 wt%), the surface roughness increases significantly, and the nanoparticles are more densely packed, leading to a more heterogeneous morphology (Figure 5c). The formation of distinct phases (illuminated and dark zones) in the SEM images suggests the presence of both epoxy-rich and nanoparticle-rich regions, which aligns with the XRD results showing the formation of calcium silicate (Ca_3SiO_5) and hydration products. The increased surface roughness and heterogeneous morphology at higher cement content contribute to the enhanced mechanical properties (e.g., hardness, impact strength) and thermal insulation of the composites. The improved interfacial adhesion and uniform dispersion of nanoparticles are critical for achieving optimal performance in building construction applications.

3.2. Mechanical Properties

The hardness test is commonly used to evaluate material indentation using an indenter made of diamond or steel with a specific force and geometry. The findings of Shore D hardness tests show that increasing the cement content in the composite leads to a gradual increase in hardness, as shown in Figure 6a. In the present work, the Shore D hardness of epoxy is 80 MPa, which is higher than those reported (~68 MPa) [7]. The difference between the two hardness values for epoxy could be related to the varied ratio of epoxy to hardener, as the ratio in the previous study was 3:1, compared to 2:1 in this investigation. Hardness values are improved for all epoxy–cement composites, which could be attributed to the greater cross-linking and stacking [28], thus restricting the movement of polymer molecules and leading to increased scratching and cutting resistance. Composites are also more resistant to plastic deformation since material hardness is a measure of the forces between atoms or molecules in the material; stronger connections improve the hardness value [61]. Shore D hardness increases with an increase in cement ratio in epoxy–cement composites, similar to the addition of other fillers such as copper and graphene nanoparticles. However, the hardness increases by a greater factor for the cement ratio than for copper and graphene fillers [39].

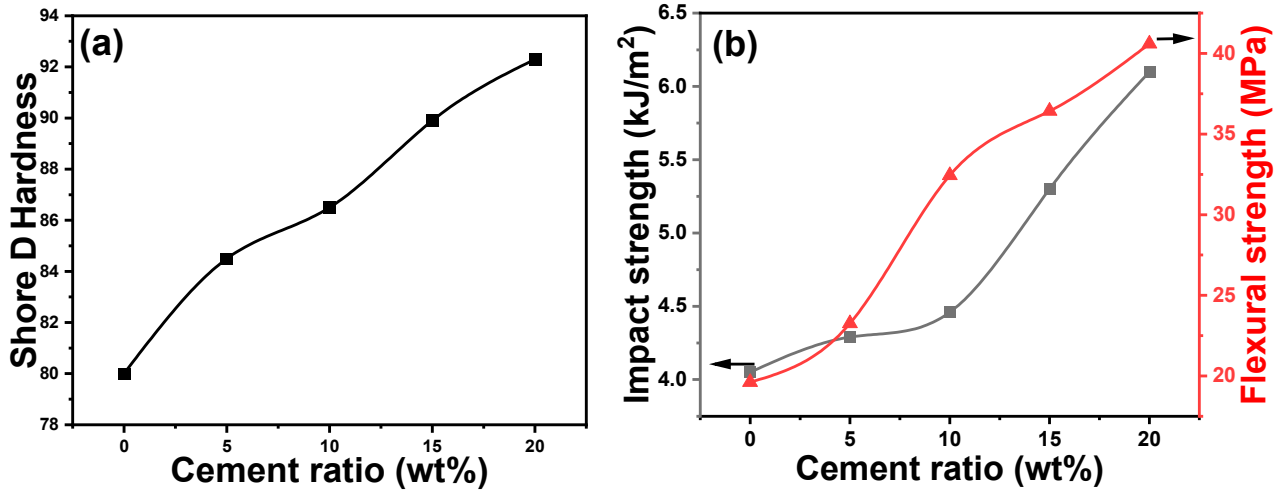


Figure 6. (**a**) Shore D hardness and (**b**) impact/flexural strength versus cement ratio of epoxy–cement composites.

Figure 6b shows the impact strength and flexural strength versus cement ratio of epoxy–cement composites. Matrix composites exhibited a considerable increase in impact energy with the insertion of 20 wt% cement, as shown in Figure 6b. The increase in impact energy could be ascribed to the good interfacial adhesion between the epoxy and cement nanoparticles, which increases the impact energy and, therefore, improves the impact strength (I.S.) [62]. However, flexural strength (σ) is defined by the amount of indirect tension or stress that concrete must withstand. The behavior of σ versus cement ratio is similar to the behavior of I.S., and it is usually attributed to polymer concrete formulations. The highest value of σ is 40.6 MPa for the epoxy-20 wt% cement composite, which is two times larger than the σ of epoxy ordinary concrete (19.61 MPa). Knowing the value of σ allows us to build seamless structural components like shafts, beams, and cantilevers. It can also be used to forecast the durability of raw materials and structures [63,64]. The value of σ for epoxy–cement composites slightly increased with the cement ratio elsewhere, with the greatest flexural strength reported as ~15 MPa at a cement ratio of 16 wt%, compared to ~37 MPa in the current work [23]. Polymer concrete is a composite material in which polymeric components are used to bind the aggregates, just like Portland cement concrete. Generally, the applied load immediately reduces when failure occurs [17]. The observed result can be explained by the greater aggregate size, which reduces voids in the composite (making it denser) and hence increases σ [65,66].

3.3. Thermal Conductivity

Figure 7 depicts the thermal conductivity (K) of epoxy–cement composites. The value of K decreases as the cement ratio increases up to 20 wt%. The behavior of K indicates that the thermal insulation of epoxy improves as the cement ratio increases. This is because the polymer may establish an interface between the cement fillers [67,68]. The thermal conductivity of epoxy–cement composites varies (increases or decreases without a clear trend) with the cement ratio, but there is a clear trend between K and the composite's porosity, which decreases as porosity increases [23]. The additional increase in the cement ratio in the epoxy–cement composite may reduce the value of K, as seen elsewhere where the value of K approaches less than ~0.07 W/m·K for a cement ratio of ~90 wt% (epoxy ratio ~10 wt%) [40]. Although the thermal conductivity of pure cement was not measured in this study, we recognize that such data would offer valuable context for interpreting the findings. Generally, the thermal conductivity of OPC typically ranges from 0.8 to 1.5 W/m·K, which is notably higher than that of epoxy resin. The observed reduction in thermal conductivity

with increasing cement content could be explained by the presence of air voids, resulting in interfacial thermal resistance between the epoxy matrix and cement particles.

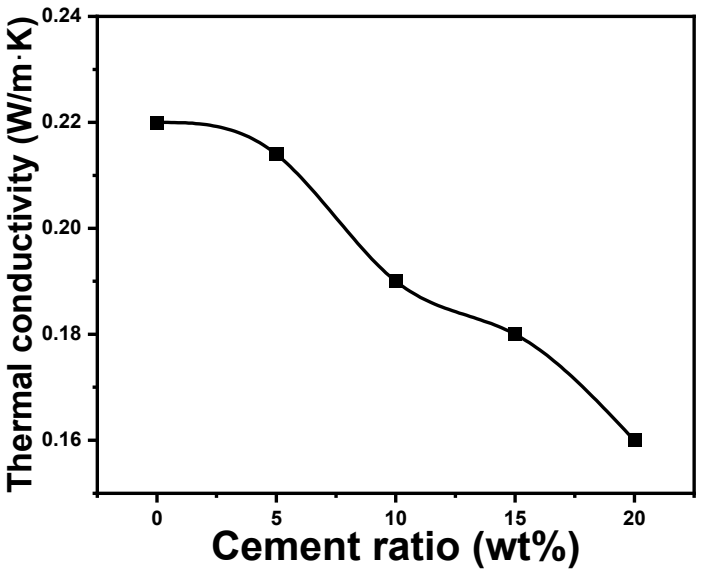


Figure 7. Thermal conductivity versus cement ratio for epoxy–cement composites.

Other fillers, such as date palms, have been used to decrease the thermal conductivity of epoxy or increase its thermal insulation [14]. For example, the value of K decreased from 0.26 to 0.15 W/m·K when the date palm ratio in the epoxy composites was increased to 30 wt%. The effects of cement on the thermal conductivity coefficient and permeability of epoxy–cement composites have been investigated [38]. Polymer–mortar composites have a K of 0.6 W/m·K for 30 wt% polymers. The K of epoxy was improved to 0.449 W/m·K by incorporating 3 wt% silicon carbide nanowires, which is 1.06 times higher than that of pure epoxy [38]. Also, the K of epoxy has been improved and reached 0.2 W/m·K with the addition of 25 wt% nettle fiber [69]. However, epoxy resin–concrete composites are a new category of concrete that possesses high strength, fast development strength, good toughness, short forming time, and simple construction, among other characteristics [70]. It also performs well in terms of abrasion resistance, water resistance, chemical corrosion resistance, and freeze resistance [71]. Therefore, it can be employed in a wide range of practical engineering fields, such as building construction [24].

As listed in Table 2, the roughness of epoxy is 2.71 μm, but it gradually increased with cement concentrations until it reached 6.21 μm at 0.20 wt%. This behavior may be related to the ability of the epoxy surface to hold more nanoparticles with larger visible agglomerates, causing the epoxy surface to be covered with large agglomerates, resulting in high roughness [72,73]. As seen in Figure 8, the WCA gradually increased from about 81.61° to 89.52° as the wt% of cement increased to 10%, but it rose above 90° (92.61° and 98.87°) when the wt% of cement exceeded 15%. Similar values are also listed in Table 2. This indicates that the epoxy became more hydrophobic, and the wettability of the surface decreased, such that ϕ and wettability should have an inverse relationship. Moreover, it can easily shed dust and could be used in self-cleaning glass fabrication [74]. Smaller WCAs or larger spreading areas imply higher wettability because the surface area (SA) is expected to increase with roughness (the real SA is higher than the geometrical SA). Therefore, wettability and roughness are strongly related, but the wetting characteristics of SA depend strongly on the nanoparticle distribution within the surface layers [75–77]. The equation is as follows: $(1+\cos\theta_i)\gamma_{LS} = 2(\sqrt{\gamma_L^D\gamma_S^D} + \sqrt{\gamma_L^P\gamma_S^P})$, where L and S refer to the liquid and solid surfaces, respectively. D and P represent the London dispersion

force and polar dispersion force, respectively. However, Kennedy et al. and Roberson et al. converted WCA to surface energy using the following relation [77–79]: $\gamma = 74.5 - 0.372\ WCA - 0.00181 \times WCA^2$.

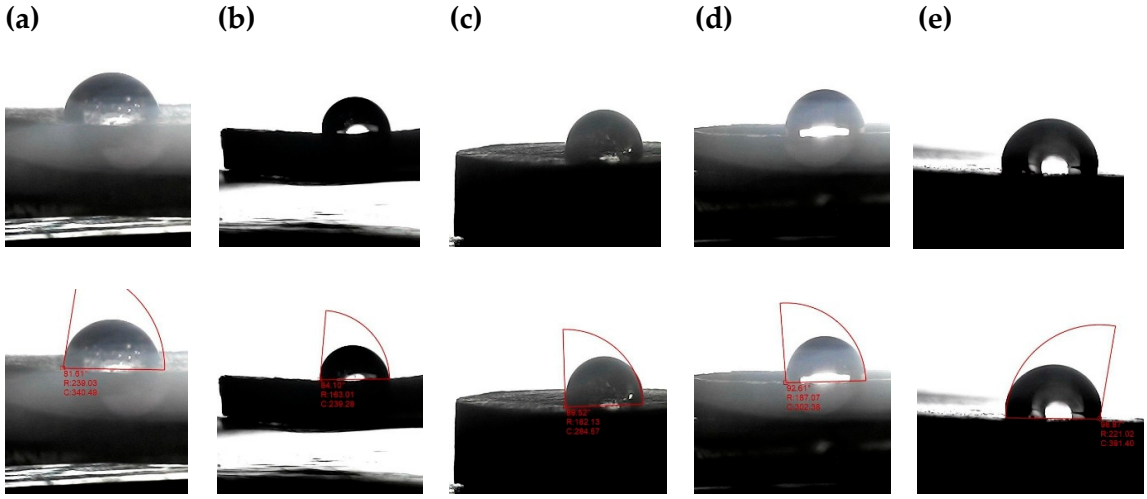


Figure 8. WCA image on the surface of (**a**) pure epoxy and epoxy/cement nanocomposites containing (**b**) 5 wt%, (**c**) 10 wt%, (**d**) 15 wt%, and (**e**) 20 wt% cement.

Table 2. Roughness, WCA, and surface energy (γ) of pure epoxy and epoxy/cement nanocomposites.

Samples	Roughness (μm)	WCA (°)	γ (Dyne/cm)
Epoxy	2.71	81.61	32.09
Epoxy + 5 wt% cement	3.54	84.10	30.41
Epoxy + 10 wt% cement	5.10	89.52	26.69
Epoxy + 15 wt% cement	5.84	92.61	25.67
Epoxy + 20 wt% cement	6.21	98.87	20.03

The values of γ listed in Table 2 are inversely proportional to roughness and WCA. The rough surface increases the WCA but decreases γ, such that a smaller area of the composite is in contact with water. In general, lowering γ and creating a rough surface can produce a suitable hydrophobic surface on a smooth substrate. Water vapor molecules can interact significantly with hydrophobic moieties when an active photocatalyst is properly constructed, and a large proportion of its surface is covered with hydrophobic materials. The surface can repel water droplets [80,81]. It has been stated that the hydrophobicity of the surface is influenced by the type of matrix and the composition of the filler constituents [82]. In fact, it was expected that as roughness increases, the WCA should also increase, as explained by the lotus effect, whereby lotus leaves repel water due to the presence of small bumps at the micro- and nanometer scales on the surface [83,84]. In this case, a drop of water is supported between the peaks of the protuberances, which provides the shortest contact, thus acquiring a more spherical shape (i.e., with a higher WCA).

Cement nanoparticles enhance the hydrophobicity of epoxy composites, leading to an increase in WCA. The incorporation of cement nanoparticles increases the surface roughness of the epoxy composite. According to the Cassie–Baxter model, a rough surface traps air pockets beneath water droplets, reducing the contact area between the water and the solid surface [46,47]. This results in a higher WCA and increased hydrophobicity. Cement nanoparticles introduce elements such as calcium, silicon, and aluminum, which can form hydrophobic compounds or coatings on the surface. These compounds reduce the surface energy of the composite, making it less wettable and increasing the WCA. The

uniform distribution of cement nanoparticles creates a micro- and nano-scale texture on the surface, further enhancing hydrophobicity. This texture mimics the lotus effect, where water droplets bead up and roll off the surface, carrying away dirt and contaminants.

The improvement in WCA can be explained by the formation of a rough surface. Cement nanoparticles create a hierarchical surface structure with micro- and nano-scale features. This roughness reduces the contact area between water droplets and the surface, increasing the WCA. The chemical interaction between the epoxy matrix and cement nanoparticles lowers the surface energy of the composite. A lower surface energy results in weaker adhesion between water molecules and the surface, leading to a higher WCA. The rough surface traps air pockets beneath water droplets, as described by the Cassie–Baxter model [46,47]. These air pockets minimize the contact area and enhance the hydrophobic properties of the surface. The increased WCA and hydrophobicity of epoxy–cement composites make them suitable for applications such as self-cleaning surfaces; water droplets roll off the surface, carrying away dirt and contaminants. The water-resistant coatings could improve resistance to water penetration, enhancing the durability of building materials. In addition, reduced water contact minimizes the risk of corrosion in structural components.

The percentages of cement nanofillers (5, 10, 15, and 20 wt%) were selected based on the following considerations. Lower percentages (5–20 wt%) ensure uniform dispersion of cement nanoparticles within the epoxy matrix, avoiding agglomeration and maintaining homogeneity. Preliminary studies and literature suggest that these percentages provide a balance between enhancing mechanical properties (e.g., hardness, impact strength) and maintaining the structural integrity of the composite [85]. Thermal and surface properties: The selected range allows for significant improvements in thermal insulation and hydrophobicity without compromising other material properties. Higher percentages of cement nanoparticles may lead to processing challenges, such as increased viscosity and difficulty in mixing, which could affect the quality of the final composite.

While this study focused on cement percentages up to 20 wt%, we acknowledge the importance of exploring higher percentages. Based on the observed trends and literature, we anticipate the following outcomes if the cement content exceeds 20 wt%. The hardness of epoxy–cement composites is expected to continue increasing with higher cement content due to greater cross-linking and stacking of nanoparticles, which restrict polymer chain movement. However, beyond a certain threshold (e.g., 25–30 wt%), the hardness may plateau or decrease due to nanoparticle agglomeration, which can create stress concentration points and reduce overall mechanical performance. Impact strength may initially improve with higher cement content due to enhanced interfacial adhesion between the epoxy matrix and cement nanoparticles. At very high percentages (e.g., >30 wt%), the impact strength could decline due to increased brittleness and reduced flexibility of the composite. The thermal insulation properties may further improve with higher cement content, but excessive filler loading could lead to the formation of thermal bridges, reducing insulation efficiency. Hydrophobicity and surface roughness are likely to increase, but excessive cement content may lead to uneven surfaces and reduced coating performance. To address these possibilities, we plan to conduct further studies exploring higher cement percentages (e.g., up to 30–40 wt%) and their effects on the mechanical, thermal, and surface properties of epoxy–cement composites. This will provide a more comprehensive understanding of the optimal filler content for various applications.

4. Conclusions

The structural, mechanical, and thermal insulation properties of epoxy–cement composites with varying cement ratios were investigated. Key findings include:

- The structure transitioned from amorphous (pure epoxy) to crystalline (epoxy–cement composites). Cement addition hindered crack propagation, with distinct interfaces between the cement and epoxy matrix visible.
- Increasing the cement ratio up to 20 wt% led to gradual improvements in Shore D hardness, impact strength, flexural strength, and thermal insulation. The addition of fine cement fillers (up to 20 wt%) enhanced molecular compaction, improving mechanical resistance and thermal insulation by approximately four-fold compared to Portland cement concrete.
- The epoxy–cement blend exhibited excellent mechanical and thermal insulation properties, making it highly suitable for building construction applications. The incorporation of cement nanoparticles significantly improved the Shore D hardness, impact strength, and flexural strength of epoxy composites. These improvements make epoxy–cement composites suitable for structural applications in building construction, such as beams, columns, and coatings, where high mechanical performance is critical.
- The thermal conductivity of epoxy–cement composites decreased with increasing cement content, indicating enhanced thermal insulation. This property is beneficial for energy-efficient building materials, reducing heat transfer and improving energy savings.
- The WCA increased with cement content, demonstrating improved hydrophobicity. The hydrophobic nature of the composites makes them ideal for water-resistant coatings, self-cleaning surfaces, and anti-corrosion applications in construction.
- SEM and EDS analysis confirmed the uniform dispersion of cement nanoparticles and strong interfacial adhesion with the epoxy matrix. This ensures the structural integrity and durability of the composites, making them reliable for long-term use in harsh environments.
- XRD analysis revealed a low-crystalline nature for epoxy–cement composites, with the formation of calcium silicate (Ca_3SiO_5) and hydration products. This microstructure contributes to the material's mechanical and thermal properties, enhancing its overall performance.

Author Contributions: Conceptualization, S.M.J., N.A.A., S.I.H., A.A.B., N.S.A.E.-G. and A.M.A.-E.; methodology, S.M.J., N.A.A., S.I.H., A.A.B. and N.S.A.E.-G.; software, A.M.M. and A.M.A.-E.; validation, A.A.B., A.S., A.M.M. and A.M.A.-E.; formal analysis, S.M.J., N.A.A., S.I.H., A.A.B., N.S.A.E.-G., A.S., A.M.M. and A.M.A.-E.; investigation, S.M.J. and N.A.A.; resources, S.M.J.; data curation, N.A.A. and S.I.H.; writing—original draft preparation, S.M.J., N.A.A., S.I.H., N.S.A.E.-G. and A.M.A.-E.; writing—review and editing, A.S., A.M.M. and A.M.A.-E.; visualization, S.M.J. and S.I.H.; supervision, A.S., A.M.M. and A.M.A.-E.; project administration, N.A.A. and A.M.A.-E.; funding acquisition, A.A.B. and A.M.M. All authors have read and agreed to the published version of the manuscript.

Funding: The current work was assisted financially by the Dean of Science and Research at King Khalid University via the Large Group Project under grant number RGP. 2/591/45.

Institutional Review Board Statement: Not applicable.

Data Availability Statement: The original contributions presented in the study are included in the article; further inquiries can be directed to the corresponding author.

Acknowledgments: The authors extend their appreciation to the Deanship of Scientific Research at King Khalid University for funding this work through the Large Groups Project under grant number RGP.2/591/45.

Conflicts of Interest: The authors declare no conflicts of interest.

References

1. Rashad, M.; Abd-Elnaiem, A.M.; Hanafy, T.A.; Shaalan, N.M.; Shamekh, A.M.A. Optical properties of functional Al_2O_3 nano-filler in eco-friendly PVA polymer for flexible optoelectronic devices. *Opt. Mater.* **2023**, *141*, 113990. [CrossRef]
2. Zhang, S.; Zhang, H.; Jia, Z.; Cao, R.; Xiong, Y.; Chen, C.; Zhang, Y. Thermal properties of amino-functionalized multi-walled carbon nanotubes reinforced epoxy-based transducers embedded in concrete. *Cem. Concr. Compos.* **2022**, *127*, 104411. [CrossRef]
3. Lokuge, W.; Aravinthan, T. Effect of fly ash on the behaviour of polymer concrete with different types of resin. *Mater. Des.* **2013**, *51*, 175–181. [CrossRef]
4. Prabakaran, E.; Kumar, D.V.; Jaganathan, A.; Kumar, P.A.; Veeerapathran, M. Analysis on Fiber Reinforced Epoxy Concrete Composite for Industrial Flooring–A Review. *J. Phys. Conf. Ser.* **2022**, *2272*, 012026. [CrossRef]
5. Mercante, I.; Alejandrino, C.; Ojeda, J.P.; Chini, J.; Maroto, C.; Fajardo, N. Mortar and concrete composites with recycled plastic: A review. *Sci. Technol. Mater.* **2018**, *30*, 69–79. [CrossRef]
6. Mohammed, T.; Rahmah, N.; Jawad, L. Thermal properties of nano-composites: A comparative study between epoxy/graphene and epoxy/$CaCO_3$. *J. Eng. Sci. Technol.* **2023**, *18*, 424–436.
7. Mohammed Ali, A.N.; Ali, N.A.; Hussein, S.I.; Hakamy, A.; Raffah, B.; Alofi, A.S.; Abd-Elnaiem, A.M. Nanoarchitectonics of silver/poly (methyl methacrylate) films: Structure, optical characteristics, antibacterial activity, and wettability. *J. Inorg. Organomet. Polym. Mater.* **2023**, *33*, 694–706. [CrossRef]
8. Abd-Elnaiem, A.M.; Hussein, S.I.; Assaedi, H.S.; Mebed, A.M. Fabrication and evaluation of structural, thermal, mechanical and optical behavior of epoxy–TEOS/MWCNTs composites for solar cell covering. *Polym. Bull.* **2021**, *78*, 3995–4017. [CrossRef]
9. Hassani Niaki, M.; Fereidoon, A.; Ghorbanzadeh Ahangari, M. Mechanical properties of epoxy/basalt polymer concrete: Experimental and analytical study. *Struct. Concr.* **2018**, *19*, 366–373. [CrossRef]
10. Zeng, X.; Zhang, Z.; Pan, Y.; Zhang, Y.; Hou, L. Epoxy-based composites with enhanced thermal properties through collective effect of different particle size fillers. *Polym. Polym. Compos.* **2022**, *30*, 09673911221106686. [CrossRef]
11. Benega, M.A.G.; Silva, T.F.; Santos, S.F. Improvements in thermal and mechanical properties of composites based on epoxy-carbon nanomaterials: A brief landscape. *Polym. Test.* **2021**, *98*, 107180. [CrossRef]
12. Zhou, H.; Brooks, A.L. Thermal and mechanical properties of structural lightweight concrete containing lightweight aggregates and fly-ash cenospheres. *Constr. Build. Mater.* **2019**, *198*, 512–526. [CrossRef]
13. Dagdag, O.; Benhiba, F.; Guenbour, A.; Bellaouchou, A.; Hajjaji, N.; Jama, C.; Zarrouk, A. Study on thermal conductivity and mechanical properties of cyclotriphosphazene resin-forced epoxy resin composites. *Crystals* **2023**, *13*, 478. [CrossRef]
14. Ghazi, I.F.; Jaddan, R.I. Thermal conductivity characterization of epoxy-based composites reinforced with date palm waste particles. *J. Phys. Conf. Ser.* **2021**, *1973*, 012144. [CrossRef]
15. Janjaroen, T.; Panitchanit, C.; Kaewthai, N.; Boonserm, K.; Sanawung, A.; Pakawanit, P. The mechanical and thermal properties of cement CAST mortar/graphene oxide composites materials. *Int. J. Concr. Struct. Mater.* **2022**, *16*, 34. [CrossRef]
16. Colangelo, F.; Roviello, G.; Ricciotti, L.; Ferrandiz-Mas, V.; Messina, F.; Ferone, C.; Tarallo, O.; Cioffi, R.; Cheeseman, C.R. Mechanical and thermal properties of lightweight geopolymer composites. *Cem. Concr. Compos.* **2018**, *86*, 266–272. [CrossRef]
17. Golestaneh, M.; Amini, G.; Najafpour, G.D.; Beygi, M.A. Evaluation of mechanical strength of epoxy polymer concrete with silica powder as filler. *World Appl. Sci. J.* **2010**, *9*, 216–220.
18. Mao, L.; Barnett, S.J.; Tyas, A.; Warren, J.; Schleyer, G.K.; Zaini, S.S. Response of small-scale ultra-high performance fibre reinforced concrete slabs to blast loading. *Constr. Build. Mater.* **2015**, *93*, 822–830. [CrossRef]
19. Behfarnia, K.; Behravan, A. Application of high-performance polypropylene fibers in concrete lining of water tunnels. *Mater. Des.* **2014**, *55*, 274–279. [CrossRef]
20. Wang, W.; Shen, A.; Lyu, Z.; He, Z.; Nguyen, K.T.Q. Fresh and rheological characteristics of fiber reinforced concrete—A review. *Constr. Build. Mater.* **2021**, *296*, 123734. [CrossRef]
21. Shi, J.; Chen, D.; Yu, Z. Novel epoxy resin-bonded sand system: Mechanical strength, deterioration resistance, and failure mechanism. *Eng. Fail. Anal.* **2024**, *158*, 108020. [CrossRef]
22. Hussein, S.I.; Abd-Elnaiem, A.M.; Asafa, T.B.; Jaafar, H.I. Effect of incorporation of conductive fillers on mechanical properties and thermal conductivity of epoxy resin composite. *Appl. Phys. A* **2018**, *124*, 475. [CrossRef]
23. Elalaoui, O.; Ghorbel, E.; Mignot, V.; Ben Ouezdou, M. Mechanical and physical properties of epoxy polymer concrete after exposure to temperatures up to 250 °C. *Constr. Build. Mater.* **2012**, *27*, 415–424. [CrossRef]
24. Abd-Elnaiem, A.M.; El-Aziz, M.A.; Hassan, A.I.; Shalaby, T.A.; Al-Kahtani, A.M. Ameliorating the mechanical parameters, thermal stability, and wettability of acrylic polymer by cement filling for high-efficiency waterproofing. *Polymers* **2022**, *14*, 4671. [CrossRef] [PubMed]
25. Abd-Elnaiem, A.M.; El-Aziz, M.A.; Hassan, A.I.; Shalaby, T.A.; Al-Kahtani, A.M. Mechanical characteristics and thermal stability of hybrid epoxy and acrylic polymer coating/nanoclay of various thicknesses. *J. Inorg. Organomet. Polym. Mater.* **2022**, *32*, 2094–2102. [CrossRef]

26. Sivasankar, S.; Dhal, L.; Gopalakrishnan, R.; Velrajkumar, G.; Jose, A. Strength and ductility of reinforced concrete using basalt fibre-reinforced polymers. *Polym. Bull.* **2024**, *81*, 6473–6493. [CrossRef]
27. Wang, R.; Shi, X.X.; Wang, P.M. Recent research on polymer-modified cement mortar in China. *Adv. Mater. Res.* **2013**, *687*, 57–67. [CrossRef]
28. Łukowski, P. Studies on the microstructure of epoxy-cement composites. *Arch. Civ. Eng.* **2016**, *62*, 101–113. [CrossRef]
29. Song, Y.; Chunmei, Z.; Xiaowei, C.; Xiaoyang, G. Modification of toughness of oil well cement by plasma modified rock asphalt. *Bull. Chin. Ceram. Soc.* **2016**, *35*, 4082–4087. [CrossRef]
30. Papanicolaou, G.C.; Anastasiou, D.E. Development of environmentally friendly epoxy and composite adhesives and applications in single and mixed-modulus joints. *J. Adhes. Sci. Technol.* **2021**, *35*, 1138–1153. [CrossRef]
31. Ferrari, F.; Lotti, N.; Celli, A.; Bonetti, F.; D'Urso, L.; Malucelli, G. Fully recyclable bio-based epoxy formulations using epoxidized precursors from waste flour: Thermal and mechanical characterization. *Polymers* **2021**, *13*, 2768. [CrossRef] [PubMed]
32. Ming, L.I.; Zhang, J.; Wang, H.; Liu, Y.; Xie, S. Mechanical properties of oil well cement stone reinforced with hybrid fiber of calcium carbonate whisker and carbon fiber. *Petrol. Explor. Dev.* **2015**, *42*, 104–111. [CrossRef]
33. Chen, X.; Chen, S.; Xu, Z.; Zhang, J.; Miao, M.; Zhang, D. Degradable and recyclable bio-based thermoset epoxy resins. *Green Chem.* **2020**, *22*, 4187–4198. [CrossRef]
34. Li, J.; Xie, J.; Liu, F.; Lu, Z. A Critical Review and Assessment for FRP-Concrete Bond Systems with Epoxy Resin Exposed to Chloride Environments. *Compos. Struct.* **2019**, *229*, 111372. [CrossRef]
35. Chung, S.-L.; Lin, J.-S. Thermal conductivity of epoxy resin composites filled with combustion synthesized h-BN particles. *Molecules* **2016**, *21*, 670. [CrossRef]
36. Jaafar, H.I. Effect of SiC particles and water absorption on thermal conductivity of epoxy reinforcement by (bi-directional) glass fiber. *Iraqi J. Phys.* **2011**, *9*, 13–17.
37. Shen, D.; Zhan, Z.; Liu, Z.; Cao, Y.; Zhou, L.; Liu, Y.; Dai, W.; Zhang, Y. Enhanced thermal conductivity of epoxy composites filled with silicon carbide nanowires. *Sci. Rep.* **2017**, *7*, 2606. [CrossRef]
38. Matlk, B.M.; Fahad, B.M.; Ghalib, L. Effect of epoxy addition on thermal conductivity, expansion, and permeability of cement mortar. *J. Eng. Sustain. Dev.* **2020**, *24*, 388–394. [CrossRef]
39. Ali, N.A.; Aljohani, N.R.; Alshahrani, S.M.; Zaki, F.H.; Khan, A. Thermal and mechanical properties of epoxy resin functionalized copper and graphene hybrids using in-situ polymerization method. *Curr. Nanosci.* **2021**, *17*, 494–502. [CrossRef]
40. Jiang, J.; Lu, Z.; Niu, Y.; Li, J. Investigation of the properties of high-porosity cement foams containing epoxy resin. *Constr. Build. Mater.* **2017**, *154*, 115–122. [CrossRef]
41. Viapiana, R.; Smaniotto, A.; Martins, L.M.; Monteiro, M.G.; Parizotto, N.A.; Oliveira, P.T.; Petzhold, C.L. Chemical characterization and bioactivity of epoxy resin and Portland cement-based sealers with niobium and zirconium oxide radiopacifiers. *Dent. Mater.* **2014**, *30*, 1005–1020. [CrossRef] [PubMed]
42. Sarathi, R.; Sahu, R.K.; Rajeshkumar, P. Understanding the thermal, mechanical and electrical properties of epoxy nanocomposites. *Mater. Sci. Eng. A* **2007**, *445*, 567–578. [CrossRef]
43. Ranella, A.; Barberoglou, M.; Bakogianni, S.; Fotakis, C.; Stratakis, E. Tuning cell adhesion by controlling the roughness and wettability of 3D micro/nano silicon structures. *Acta Biomater.* **2010**, *6*, 2711–2720. [CrossRef] [PubMed]
44. Conradi, M.; Kocijan, A. Fine-tuning of surface properties of dual-size TiO_2 nanoparticle coatings. *Surf. Coat. Technol.* **2016**, *304*, 486–491. [CrossRef]
45. Wassmann, T.; Seitz, M.; Müller, P.; Winter, M.; Dvorak, J.; Moser, J.; Hellwig, E. The influence of surface texture and wettability on initial bacterial adhesion on titanium and zirconium oxide dental implants. *Int. J. Implant Dent.* **2017**, *3*, 32. [CrossRef] [PubMed]
46. Dowling, D.P.; Miller, I.S.; Ardhaoui, M.; Gallagher, W.M. Effect of surface wettability and topography on the adhesion of osteosarcoma cells on plasma-modified polystyrene. *J. Biomater. Appl.* **2011**, *26*, 327–334. [CrossRef]
47. Sarathi, R.; Sahu, R.K.; Tanaka, T. Understanding the hydrophobic characteristics of epoxy nanocomposites using wavelets and fractal technique. *IEEE Trans. Dielectr. Electr. Insul.* **2008**, *15*, 178–186. [CrossRef]
48. Zavrl, E.; El Mankibi, M.; Dovjak, M.; Stritih, U. Enhancing performance of building elements with phase change materials for cooling with air-based systems. *J. Energy Storage* **2022**, *51*, 104461. [CrossRef]
49. Daghash, S.M.; Soliman, E.M.; Kandil, U.F.; Taha, M.M.R. Improving impact resistance of polymer concrete using CNTs. *Int. J. Concr. Struct. Mater.* **2016**, *10*, 539–553. [CrossRef]
50. Ary Subagia, I.D.G.; Kim, Y. A study on flexural properties of carbon-basalt/epoxy hybrid composites. *J. Mech. Sci. Technol.* **2013**, *27*, 987–992. [CrossRef]
51. Raju, G.U.; Gaitonde, V.N.; Kumarappa, S. Experimental study on optimization of thermal properties of groundnut shell particle reinforced polymer composites. *Int. J. Emerg. Sci.* **2012**, *2*, 433–454. [CrossRef]
52. ElSafty, A.; Abdel-Mohti, A. Investigation of likelihood of cracking in reinforced concrete bridge decks. *Int. J. Concr. Struct. Mater.* **2013**, *7*, 79–93. [CrossRef]

53. Greco, A.; Esposito Corcione, C.; Maffezzoli, A. Effect of multi-scale diffusion on the permeability behavior of intercalated nanocomposites. *J. Membr. Sci.* **2016**, *505*, 92–99. [CrossRef]
54. Jo, Y.K.; Do, J. Hardening properties of epoxy-modified cement composites without hardener. *Polymers Polymer Compos.* **2016**, *24*, 195–204. [CrossRef]
55. Doumeng, M.; Makhlouf, L.; Berthet, F.; Marsan, O.; Delbé, K.; Denape, J.; Chabert, F. A comparative study of the crystallinity of polyetheretherketone by using density, DSC, XRD, and Raman spectroscopy techniques. *Polym. Test.* **2021**, *93*, 106878. [CrossRef]
56. Seo, Y.; Kim, S.-M. Longitudinal cracking at transverse joints caused by dowel bars in Jointed Concrete Pavements. *KSCE J. Civ. Eng.* **2013**, *17*, 395–402. [CrossRef]
57. Li, Y.; Guo, Y.; Lyu, Z.; Wei, X. Investigation of the effect of waterborne epoxy resins on the hydration kinetics and performance of cement blends. *Constr. Build. Mater.* **2021**, *301*, 124045. [CrossRef]
58. Reis, J.M.L. Fracture and flexural assessment of red mud in epoxy polymer mortars. *Mater. Struct.* **2015**, *48*, 3929–3936. [CrossRef]
59. Shen, F.; Huang, S.; Sun, Z.; Ding, Q. Research on Hardening Mechanism of Cement-Emulsified Asphalt-Epoxy Resin. *Adv. Mater. Res.* **2012**, *430–432*, 434–437. [CrossRef]
60. Sasaki, I.; Nishizaki, I. Study on the durability of surface coating materials for concrete structures. *City* **2008**, *305*, 8516.
61. Zhong, W.; Wu, Y. Influence of damage degree on self-healing of concrete. *Constr. Build. Mater.* **2008**, *22*, 1137–1142. [CrossRef]
62. Peiyu, Y.; Lei, Y.; Dan, D.; Yuwei, L. Effect of epoxy resin on the hydration and mechanical property of oil well cement stone. *Bull. Chin. Ceram. Soc.* **2016**, *35*, 2019–2023. [CrossRef]
63. Rajab, M.A.; Kader, E.I.; Hammod, A.A.; Hameed, A.H.I. Mechanical properties (Tensile, Hardness, and Shock resistance) for the phenol formaldehyde resin with epoxy resin. *Diyala J. Eng. Sci.* **2019**, *15*, 35–43. [CrossRef]
64. Girimurugan, R.; Pugazhenthi, R.; Maheskumar, P.; Suresh, T.; Vairavel, M. Impact and hardness behaviour of epoxy resin matrix composites reinforced with banana fiber/camellia sinensis particles. *Mater. Today Proc.* **2021**, *39*, 373–377. [CrossRef]
65. Siva, R.; Kesavaram, B.; Martin, J.J.; Mathiselvan, G.; Navas, K.B.; Sangeetha, M. Mechanical behavior of sisal and banana fiber reinforced hybrid epoxy composites. *Mater. Today Proc.* **2021**, *44*, 3692–3696. [CrossRef]
66. Smirnov, S.; Konovalov, D.; Veretennikova, I.; Pestov, A.; Smirnova, E. Effect of modifying dopes on the mechanical properties of epoxy coatings affected by thermocycling. *Procedia Struct. Integr.* **2020**, *25*, 209–213. [CrossRef]
67. Oleiwi, J.K.; Abass, B.A. Thermal Properties of Polymeric Composites Reinforced by Nanoceramic Materials. *Int. J. Mech. Prod. Eng. Res. Dev.* **2018**, *8*, 517–524. [CrossRef]
68. Edaan, G.E. Measurement of Thermal Conductivity of Epoxy Resin Reinforced With Different Weight Ratios of Glass and Carbon Powders. *Al-Bahir J. Eng. Pure Sci.* **2023**, *3*, 5. [CrossRef]
69. Suarsana, K.; Putra Negara, D.N.K.; Suryawan, I. Properties of Thermal Conductivity Hybrid Epoxy Resin Composite Reinforced Natural Fiber as Alternative Insulator Material. *Teknik* **2023**, *43*, 264–271. [CrossRef]
70. Pi, Z.; Xiao, H.; Du, J.; Liu, M.; Li, H. Interfacial microstructure and bond strength of nano-SiO_2-coated steel fibers in cement matrix. *Cem. Concr. Compos.* **2019**, *103*, 1–10. [CrossRef]
71. Dos Santos, V.; Tonoli, G.H.D.; Marmol, G.; Savastano, H., Jr. Fiber-cement composites hydrated with carbonated water: Effect on physical-mechanical properties. *Cem. Concr. Res.* **2019**, *124*, 105812. [CrossRef]
72. Kocijan, A.; Conradi, M.; Hočevar, M. The Influence of Surface Wettability and Topography on the Bioactivity of TiO2/Epoxy Coatings on AISI 316L Stainless Steel. *Materials* **2019**, *12*, 1877. [CrossRef]
73. Petrik, P.; Biró, L.P.; Fried, M.; Lohner, T.; Berger, R.; Schneider, C.; Gyulai, J.; Ryssel, H. Comparative Study of Surface Roughness Measured on Polysilicon Using Spectroscopic Ellipsometry and Atomic Force Microscopy. *Thin Solid Film.* **1998**, *315*, 186–191. [CrossRef]
74. Al-Shomar, S.M.; Barakat, M.A.Y.; Abdallah, A.W. Ellipsometric and ultrasonic studies of nano titanium dioxide specimens doped with Erbium. *Mater. Res. Express* **2020**, *7*, 106413. [CrossRef]
75. Khalil, N.Z.; Johanne, M.F.; Ishak, M. Influence of Al_2O_3 nanoreinforcement on the adhesion and thermomechanical properties for epoxy adhesive. *Compos. Part B Eng.* **2019**, *172*, 9–15. [CrossRef]
76. Hill, D.; Barron, A.R.; Alexander, S. Comparison of hydrophobicity and durability of functionalized aluminum oxide nanoparticle coatings with magnetite nanoparticles–links between morphology and wettability. *J. Colloid Interface Sci.* **2019**, *555*, 323–330. [CrossRef]
77. Jadhav, A.; Pawar, A.; Hwang, T.R.; Lee, J.W.; Choi, M.W.; Kim, B.K.; Kang, Y.S. Wavelength conversion using rare earth doped oxides in polyolefin based nanocomposite films. *Polym. Int.* **2012**, *61*, 943–950. [CrossRef]
78. Kennedy, S.B.; Washburn, N.R.; Simon, C.G., Jr.; Amis, E.J. Combinatorial screen of the effect of surface energy on fibronectin-mediated osteoblast adhesion, spreading and proliferation. *Biomaterials* **2006**, *27*, 3817–3824. [CrossRef]
79. Ashley, K.M.; Raghavan, D.; Douglas, J.F.; Karim, A. Wetting−Dewetting Transition Line in Thin Polymer Films. *Langmuir* **2005**, *21*, 10297–10305. [CrossRef]
80. Lee, J.H.; Park, E.J.; Kim, D.H.; Jeong, M.-G.; Kim, Y.D. Superhydrophobic surfaces with photo-catalytic activity under UV and visible light irradiation. *Catal. Today* **2016**, *260*, 32–38. [CrossRef]

81. Mohsin, M.M.; Ali, F.H. Enhancement of pigments hydrophobicity by mixing with Cr doped SiO_2 nanoparticles. *Chem. Methodol.* **2023**, *7*, 335–347. [CrossRef]
82. Syakur, A.; Sutanto, H. Determination of hydrophobic contact angle of epoxy resin compound silicon rubber and silica. In *Proceedings of the IOP Conference Series: Materials Science and Engineering*; IOP Publishing: Bristol, UK, 2017; Volume 190, p. 012025. [CrossRef]
83. Lafuma, A.; Quéré, D. Superhydrophobic states. *Nat. Mater.* **2003**, *2*, 457–460. [CrossRef] [PubMed]
84. Pinto, D.; Amaro, A.M.; Bernardo, L. Experimental study on the surface properties of nanoalumina-filled epoxy resin nanocomposites. *Appl. Sci.* **2020**, *10*, 733. [CrossRef]
85. Daniel, A.; Islam, M.R.; Sumdani, M.G.; Firouzi, A. Influence of Hydration on the Mechanical, Structural, Thermal, and Morphological Properties of Cement-Filled Epoxy Composites. *J. Vinyl Addit. Technol.* **2020**, *26*, 527–538. [CrossRef]

Disclaimer/Publisher's Note: The statements, opinions and data contained in all publications are solely those of the individual author(s) and contributor(s) and not of MDPI and/or the editor(s). MDPI and/or the editor(s) disclaim responsibility for any injury to people or property resulting from any ideas, methods, instructions or products referred to in the content.